AIAA-87-1953

A Numerical Study of the Effects of Curvature and Convergence on Dilution Jet Mixing

J.D. Holdeman, NASA Lewis Research Center, Cleveland, OH; R. Reynolds and C. White, The Garrett Turbine Engine Company, Phoenix, AZ

AIAA/SAE/ASME/ASEE 23rd Joint Propulsion Conference

June 29-July 2, 1987/San Diego, California

NASA Technical Memorandum 89878
AIAA-87-1953

A Numerical Study of the Effects of Curvature and Convergence on Dilution Jet Mixing

J.D. Holdeman
Lewis Research Center
Cleveland, Ohio

R. Reynolds and C. White
The Garrett Turbine Engine Co.
Phoenix, Arizona

Prepared for the
23rd Joint Propulsion Conference
cosponsored by the AIAA, SAE, ASME, and ASEE
San Diego, California, June 29—July 2, 1987

NASA

ERRATA

NASA Technical Memorandum 89878

A NUMERICAL STUDY OF THE EFFECTS OF CURVATURE
AND CONVERGENCE ON DILUTION JET MIXING

J.D. Holdeman, R. Reynolds, and C. White
February 1988

Page 12, figure 7: The labels centered over parts (a) and (c) should read J = 26.4, S/H_0 = 0.25, and D/H_0 = 0.125; the labels centered over parts (b) and (d) should read J = 6.6, S/H_0 = 0.5, and D/H_0 = 0.25.

A NUMERICAL STUDY OF THE EFFECTS OF CURVATURE AND CONVERGENCE ON DILUTION JET MIXING

J. D. Holdeman*
NASA Lewis Research Center
Cleveland, Ohio

and

R. Reynolds† and C. White‡
The Garrett Turbine Engine Co.
Phoenix, Arizona

Abstract

An analytical program has been conducted to assemble and assess a three-dimensional turbulent viscous flow computer code capable of analyzing the flow field in the transition liners of small gas turbine engines. This code is of the TEACH type with hybrid numerics, and uses the power law and SIMPLER algorithms, an orthogonal curvilinear coordinate system, and an algebraic Reynolds stress turbulence model. The assessments performed in this study, consistent with results in the literature, showed that in its present form this code is capable of predicting trends and qualitative results. The assembled code was used to perform a numerical experiment to investigate the effects of curvature and convergence in the transition liner on the mixing of single and opposed rows of cool dilution jets injected into a hot mainstream flow.

Nomenclature

C	$(S/H_0)\sqrt{J}$; Eq. (2)
D	orifice diameter
DR	density ratio = (T_m/T_j)
H_0	duct height at injection plane
J	momentum flux ratio = $(DR)R^2$
n	number of holes around can; see Eq. (5)
r	radial coordinate
R	velocity ratio = (V_j/U_m)
R_{ci}	inner radius of curvature in x-r plane
R_t	inner radius of curvature at inlet in r-z plane
S	spacing between orifices
T	temperature
T_j	jet temperature
T_m	mainstream temperature
U_m	inlet mainstream velocity
V_j	jet velocity
x	axial coordinate; = 0 at orifice centerline
y	cross stream (radial) coordinate; = 0 at injection wall
z	circumferential coordinate; = 0 at jet centerline
θ	$(T_m-T)/(T_m-T_j)$; Eq. (1)
ϕ	angle around inlet from beginning of turn (in x-r plane)

Introduction

In recent years improvements in the manufacturing technology of high temperature materials have led to emphasis on increasing the power-to-weight ratio and lowering the specific fuel consumption of aircraft gas turbine engines. To accomplish this, higher pressure and temperature levels are used in the engine cycles, and engines are shorter. As a result, the hot section components are required to operate in an increasingly severe environment.

One such component in gas turbine engines is the annular transition duct that connects the exit of the combustor to the inlet of the first-stage turbine in gas turbine engines using reverse-flow combustor configurations. A cross section schematic of this type of engine with the transition liner highlighted is shown in Fig. 1. With the current trend toward shorter engines and, therefore, shorter combustors the transition liner not only must turn the flow direction 180° but must also efficiently mix the dilution air with the hot mainstream gases. A detailed understanding of the flow field

*Senior Research Engineer, Internal Fluid Mechanics Division, Member AIAA
†Specialist Engineer, Combustion Engineering Sciences
‡Development Engineer, Combustion Advanced Technology

in the transition liner is essential to control the temperature profile entering the stator, thereby affecting durability.

Experimental investigations to characterize the three-dimensional mixing in complex geometries such as transition liners are both time consuming and expensive. This provides motivation toward numerical simulations as a time and cost effective method for evaluating candidate configurations.

The purpose of this study was to develop a computer program capable of predicting the flow in transition liners used on small reverse-flow gas turbine engines. This code was to be assembled from existing submodels which provided the best available techniques and physical modeling. Improvements were made in the geometric capability and other submodels, but it was not within the scope of this study to develop substantially different modeling techniques.

The assembled model was tested against experimental data for flows with characteristics similar to those found in transition liners[1]. This model was then used to perform the numerical experiments reported herein to assess the mixing in curved transition liners as compared with that in straight ducts[2-4].

Numerical Model

The transition mixing model is based on the three-dimensional elliptic code developed in Ref. 5. The original code contains the same numerics and physical submodels as the well-known TEACH series of codes. Since its original publication, the code has undergone several modifications to better tailor it to gas turbine combustor analyses. As part of the present study, several more features were added which are outlined briefly in the following sections.

Coordinate System

The original code was converted to a generalized orthogonal coordinate system. Since transition liners are invariably of an axisymmetric geometry, a significant simplification in the coordinate system was possible: If a global coordinate system is considered where x is coincident with the engine centerline, r is the radial distance from the engine centerline, and z is the circumferential coordinate, the transition liner curvature is confined to the x-r plane, and the liner is a body of revolution in the z direction. Thus, the general orthogonal coordinate system is required only in the x-r plane, greatly simplifying the geometry package required.

The coordinate system implementation, given in detail in Ref. 1, is based on the methods described in Refs. 6 and 7.

Numerical Scheme

The transition mixing model uses hybrid differencing, with power law blending between the central difference formulation appropriate for low convective situations and the upwind differencing scheme appropriate for high convective situations[10]. The numerical technique used is adopted from the methods described in Refs. 8 to 10 and is described in more detail in Ref. 1.

Pressure-Velocity Solution Algorithm

The SIMPLER (Semi-Implicit Method for Pressure Linked Equations Revised) method[10] is used in the current code to improve the convergence rate over that obtained with the earlier SIMPLE scheme. The implementation of this technique is given in more detail in Ref. 1.

Turbulence Model

The transition mixing model contains two turbulence models. The first is the widely used, two-equation k-ϵ model. In this model the turbulent (or effective) viscosity is determined from the solution of two additional differential equations, one for the turbulent kinetic energy, k, and the other for the turbulent dissipation rate, ϵ. The second turbulence model is an algebraic Reynolds stress (ARS) model, wherein algebraic expressions for the individual Reynolds stresses are solved to obtain an anisotropic viscosity model. The fundamental assumption in this model is that the transport of turbulence via convection and diffusion is proportional to the transport of turbulent kinetic energy. By using the transport information from the k-equation, the necessity of solving a differential equation for each Reynolds stress is eliminated, which greatly reduces both computational time and computer memory requirements.

Both models incorporate the Richardson number streamline curvature correction. The implementation of these models is described in Ref. 1. All of the calculations presented herein were performed using the algebraic Reynolds stress model.

Model Assessment

Calculations made with the code used in this study were compared with measured data for several experimental configurations having essential characteristics of transition liner flows.

Good agreement was obtained for the case of laminar flow in a square duct with a 90° bend[12], verifying that the basic numerical process was functioning correctly. Reasonable agreement was obtained for mean velocity profiles in turbulent curved duct cases[13,14] with both the k-ϵ and ARS turbulence models. The lack of any significant differences between calculations made with these models suggests that false diffusion may have been significant, masking any model differences.

Consistent with results published in the literature (e.g., Ref. 3), the scalar mixing rate predicted using the k-ϵ model is considerably less than that measured for dilution jet mixing in straight and curved ducts[15-18]. The ARS model enhances the mixing, but not to the extent indicated by the data.

A detailed discussion of the model verification and assessment performed in this study is given in Ref. 1. The principal conclusion was that the current model is capable of predicting trends and qualitative results for transition liner flows.

Description of the Flow Field

Flow and Geometry Parameters

The basic geometry for the transition liners used in the sequence of calculations performed in this study is shown in Fig. 2. The radius of curvature of the inner liner wall in the r-z plane is given nondimensionally by its ratio to the inlet channel height, R_t/H_0. The curved sections in the x-r plane were generated using circular arcs, and the curvature parameter was specified as the inner radius of curvature of the liner normalized by the inlet duct height, R_{ci}/H_0. The duct convergence was specified as the ratio of the cross-sectional area at the exit to that at the jet injection location. The primary independent flow and geometric variables, specified at the location where the dilution jets were injected into the mainstream flow, were the jet-to-mainstream momentum flux ratio, J, and the orifice spacing-to-duct height ratio, S/H_0. The orifice configurations for which calculations are presented in this paper are shown in Fig. 3. The range of variation of these independent flow and geometric variables is given in Table 1.

Table 1 Ranges of Flow and Geometric Variables Investigated

Independent variables	
Density ratio, DR	2.2
Momentum Flux Ratio, J	6.6, 26.4
Orifice Spacing, S/H_0	0.25, 0.5
Orifice Diameter, D/H_0	0.125, 0.25
Radius of Curvature in x-r plane, R_{ci}/H_0	0.25, 0.5, ∞
Radius of Curvature in r-z plane, R_t/H_0	1, 2.2, ∞
Area ration (exit/inlet)	1, 1/3

Numerical Experiments

The purpose of this study was to perform the numerical equivalent of an experimental test series to investigate the effect of the several flow and geometric parameters on the mixing process in typical transition liner geometries. In the assessment task (described in Ref. 1), it was shown that the model tended to quantitatively underpredict the mixing in the straight duct and curved channel test cases examined and would most likely do the same for transition liners. Although the prediction of absolute temperature levels was not deemed possible without further advances in numerical schemes and turbulence models, the code had demonstrated the capability to correctly predict trends, and relative comparisons between cases could therefore be made with confidence.

Most calculations were performed using a 76×28×14 grid network of 29,792 nodes, similar to that shown in Fig. 4. Plan views showing the node locations for the large and small holes, as well as the slanted slots are also shown in this figure. It was not within the scope of this study to perform detailed evaluations to establish the extent of, or to develop schemes to minimize numerical diffusion. In each case calculated, efforts were made to minimize the numerical differences by using approximately the same node spacings, so whatever numerical effects exist, they should be present in similar amounts in all cases.

The inlet duct height was 10.16 cm, and the mainstream velocity and temperature were 15 m/s and 650 K for all cases. Uniform velocity and temperature conditions were specified for both jet and mainstream inlet boundary conditions, with the inlet turbulence intensity equal to 7.5 percent of the mean velocity at jet and mainstream inlet boundaries, and the turbulence length scale equal to 2 percent of the jet diameter or inlet duct height. Neumann boundary conditions were imposed at the exit of the 180° turn.

The calculated temperature levels are presented as center-plane and cross-stream contours of the nondimensional parameter

$$\theta = (T_m - T)/(T_m - T_j) \tag{1}$$

where T is the local mean temperature, T_m is the mainstream temperature, and T_j is the jet temperature. In the following paragraphs cases are compared which differ

from each other by a single parameter, so the effect of that parameter can be examined. The flow and geometry conditions for the cases discussed are given in Table 2. The case numbers shown correspond to those in Ref. 1.

Results and Discussion

Differences Between Inner and Outer Wall Injection into a Curved Duct

Fig. 5 shows centerplane and cross-stream contour plots downstream of a row of jets injected from the inner and outer walls into a uniform mainstream flow in a nonconverging duct with a 180° turn. Orifice configuration A in Fig. 3 ($S/H_0 = 0.5$ and $D/H_0 = 0.25$) was used for these calculations with the jet-to-mainstream momentum flux ratio, J, equal to 26.4, which is an appropriate combination of orifice spacing and momentum flux ratio for optimum mixing in a straight duct[2-4]. For comparison, contours calculated for a straight duct with the same jet flow and orifice geometry are also shown in this figure. The cross-stream plots for the straight duct case are shown at downstream distances equal to the distance along the injection wall at 30° into the turn for inner and outer wall injection, respectively.

A comparison of the centerplane view of injection from the inner wall in a curved duct with that in a straight channel (Figs. 5(a) and (b)) suggests that the penetration is similar. Examination of the cross stream plots (Figs. 5(e) and (f)), however, reveals a striking difference in the structure of the jets: For inner wall injection into the curved duct, the familiar kidney shape is not evident, i.e., the minimum temperature at any radius is on the centerplane.

Figures 5(c) and (d) and 5(g) and (h) allow us to compare outer wall injection into a curved duct with injection into a straight duct. (Figs. 5(c) and (g) are from the same straight duct calculation shown in parts (b) and (f), with the plots inverted to facilitate comparison.) For outer wall injection the penetration and mixing is similar to that in a straight duct.

Table 2 Flow and Geometry Conditions

Figure	Case[a]	J	S/H_0	D/H_0	R_{ci}/H_0	R_t/H_0	Area Ratio	Configuration
5(a), (e)	9	26.4	0.5	0.25	0.5	Infinite	1	ID jets
5(b), (c), (f), (g)	12	26.4	.5	.25	Straight	-----	1	One-side
5(d), (h)	1	26.4	.5	.25	.5	Infinite	1	OD jets
6(a), (e)	1	26.4	.5	.25	.5	Infinite	1	OD jets
6(b), (c), (f)	18	26.4	1.0	.25	.5	Infinite	1	Opposed staggered
6(d), (g)	9	26.4	.5	.25	.5	Infinite	1	ID jets
7(a), (c)	37	26.4	.25	.125	.5	Infinite	1	Opposed in-line
7(b), (d)	10	6.6	.5	.25	.5	Infinite	1	Opposed in-line
8(a), (d), (e)	30	6.6	.5	.25	Straight	-----	1	Opposed in-line
8(b), (f)	10	6.6	.5	.25	.5	Infinite	1	Opposed in-line
8(c), (g)	29	6.6	.5	.25	.25	Infinite	1	Opposed in-line
9(a), (c)	21	6.6	.5	.25	Annulus	-----	1	Opposed in-line
9(b), (d)	30	6.6	.5	.25	Straight	-----	1	Opposed in-line
10(a), (d), (e)	31	6.6	.5	.25	Straight	-----	1/3	Opposed in-line
10(b), (f)	33	6.6	.5	.25	.25	Infinite	1/3	Opposed in-line
10(c), (g)	35	6.6	.5	.25	.25	2.2	1/3	Opposed in-line
11(a), (c)	41	26.4	.5	.25	Can	-----	1	One-side
11(b), (d)	12	26.4	.5	.25	Straight	-----	1	One-side
12(a), (d), (e)	38	6.6	.5	.25	Straight	-----	1	Opposed aligned slots
12(b), (f), (g)	39	6.6	.5	.25	Straight	-----	1	Opposed crossed slots
12(c), (h), (i)	30	6.6	.5	.25	Straight	-----	1	Opposed inline holes

[a]From Ref. 1

Figures 5(e) and (h) show a result observed consistently in the calculations, namely, that the structure of the inner and outer wall jets is significantly different, as the radial pressure gradient induced by the curvature inhibits the entrainment of the crossflow by the inner wall jets, and enhances that by the outer wall jets.

Opposed Rows with Jet Centerlines Staggered

It was reported in Refs. 2 to 4 that the most significant flow and geometric variables effecting the penetration and mixing of a row of jets injected into a confined crossflow were the jet-to-mainstream momentum flux ratio and the ratio of the jet spacing to the height of the duct. That is, the mixing is similar if these parameters are coupled such that

$$C = (S/H_0)\sqrt{J} \qquad (2)$$

It was shown in Ref. 3 that optimum mixing was obtained in a rectangular duct for $C \sim 2.5$ and that values of C that were a factor of 2 larger or smaller corresponded to over- and underpenetration.

It was also reported in Refs. 2 and 3 that enhanced mixing was obtained when alternate jets for optimum single-side injection were moved to the opposite wall, creating opposed rows of jets with centerlines staggered. For example, if configuration A is selected to optimize the mixing for single-side injection, then configurations B and C would be appropriate choices for opposite sides of the duct in an opposed-row staggered-jet configuration. The analogous situation in a curved duct is shown in Fig. 6. Jet centerline and cross-stream contour plots for the opposed-row configuration is shown in Figs. 6(b), (c), and (f). For comparison corresponding plots for a row of outer and inner wall jets are shown in Figs. 6(a) and (e) and 6(d) and (g), respectively.

These contours show that both the outer and inner wall jets in the opposed-row staggered-jets configuration penetrate farther than the comparable single-side case, as was also seen in the straight duct case. A difference between the cross-stream shape of the outer and inner wall jets is apparent also and is consistent with the corresponding contours of the separate outer and inner wall jet configurations.

Opposed Rows with Jet Centerlines Inline

An alternative to staggered centerlines in the opposed row configuration is to have the centerlines directly opposed. In this case the jets will impinge, and the effective mixing height is reduced to half the duct height. To maintain the appropriate ratio of orifice spacing to mixing height, the orifice spacing must also be halved[2-4]. Thus there will be four times as many injection locations, and, if the same flow split is desired, the orifice diameters must be half of that for the single-side case. This is shown in configuration D ($S/H_0 = 0.25$ and $D/H_0 = 0.125$) in Fig. 3. Centerplane and cross-stream contour plots for this configuration with $J = 26.4$ are shown in Figs. 7(a) and (c).

A lower jet-to-mainstream momentum flux ratio requires a greater orifice spacing to maintain optimum mixing, i.e., comparable penetration and mixing would be expected for $J = 6.6$ with $S/H_0 = 0.5$. Centerplane and cross-stream scalar contours for configuration A with $J = 6.6$ for opposed rows of inline jets are shown in Figs. 7(b) and (d). The similarity of the flow pattern for coupled spacing and momentum flux ratio, independent of orifice diameter, was also seen in the experimental and analytical results for opposed rows of inline jets injected into a straight duct[2,3].

These results show a tendency observed frequently in the calculations, namely, that the jet trajectories drift slightly toward the inner wall of the turn compared with where they would be in a straight duct. This was observed in the experimental results of Refs. 17 and 18 also, and is not unexpected since, in the absence of jets, the mainstream flow would establish a free vortex in the turn with radially increasing pressure and attendant inflow. The structure of the inner and outer wall jets is also strikingly different, as was observed previously for separate inner and outer wall injection.

Effects of Curvature in the x-r Plane

Figure 8 shows the effect of varying the radius of curvature. Figs. 8(b) and (f) and 8(c) and (g) are centerplane and cross-stream contours for an inner wall radius of curvature equal to ½ and ¼ the height of the inlet duct, i.e., $R_{ci}/H_0 = 0.5$ and 0.25, respectively. The jet-to-mainstream momentum flux ratio is 6.6 with an opposed-row inline jets configuration with $S/H_0 = 0.5$ and $D/H_0 = 0.25$ (configuration A). For comparison, centerplane and cross-stream contour plots for the comparable straight duct case are shown in Figs. 8(a), (d), and (e). As in previous figures, the straight and curved duct flows are similar, but the asymmetry of the mixing of the inner and outer wall jets is evident in both of the curved duct cases.

Mixing of Jets in an Annular Duct

The centerplane and cross-stream contours for a straight annulus and a comparable rectangular duct are shown in Fig. 9. The inside radius of the annulus was equal to the duct height, i.e., $R_i/H_0 = 1$. The orifice geometry was again the opposed-row inline-jets configuration A with $J = 6.6$. The similarity of the penetration and mixing as seen in both the centerplane and cross-stream contours is striking. To achieve this result, the jet spacing for the

annular duct was specified, at the radius which divides the annulus into equal areas, to be equal to that in the rectangular duct.

Convergence Effects

The effect of a 3:1 area ratio convergence in straight and curved ducts is shown in the centerplane and cross-stream contours in Fig. 10 for the opposed-row inline jets configuration. In the case of the curved duct, this convergence may be obtained through reduction in the duct height, as in the straight duct, or by circumferential convergence, if the exit annulus is at a smaller radius (closer to the engine centerline) than is the inlet. Centerplane and cross-stream scalar contours for these cases are shown in Figs. 10(b) and (f) and 10(c) and (g), respectively, and show similar distributions for all cases.

Jets Injected Into a Can

Scalar contours for jet injection into a section of a can is shown in Figs. 11(a) and (c). The jet-to-mainstream momentum flux ratio was 26.4. The jet spacing for this case was specified, at the radius which divides the can into equal areas, as that appropriate for injection of a row of jets into a rectangular duct. That is, the relationship of the spacing between jet centerlines to the number of holes around the circumference of the can would be

$$S = 2\pi R_{1/2}/n \tag{3}$$

where

$$R_{1/2} = H_0/\sqrt{2} \tag{4}$$

Substituting these into the spacing and momentum flux relationship for a rectangular duct (Eq. (2)) gives the appropriate number of holes as

$$n = \pi\sqrt{2}\,\sqrt{(J)}/C \tag{5}$$

The corresponding centerplane and cross-stream contours for the rectangular duct case are shown in Figs. 11(b) and (d), respectively.

Mixing of Jets from Slanted Slots

The final comparison to be shown is that of 2.8:1 aspect ratio slots slanted 45° to the direction of the mainstream flow in opposed-row inline jet configurations in a straight duct. These slots were examined experimentally and analytically in several straight-duct single-side-injection cases, including streamlined, bluff, and slanted-slot configurations, in Ref. 3.

In opposed-jet slanted-slot configurations the slots on opposite sides of the duct may be slanted in either the same or opposite directions. If aligned, the result is similar to that of single-side injection toward an opposite wall (as was observed previously for circular holes[2]). Centerplane and cross-stream contour plots for this case are shown in Figs. 12(a), (d), and (e) and may be compared with the corresponding plots for circular holes in Figs. 12(c), (h), and (i). The aligned-slot configuration imparts a bulk swirl to the flow consistent with the experimental results in Ref. 3. It was also reported in Ref. 3 that this configuration results in augmentation of one of the vorticies of the normal vortex pair and the supression of the other and that the jets mix less rapidly than in the circular-hole configuration. This is also evident in the calculations shown in Figs. 12(a), (d), and (e).

If the slots on opposite sides of the duct are crossed, the jet flow shifts in opposite directions in the two halves of the duct, with opposite swirl imparted on the top and bottom creating the potential for large-scale vortex interaction and high shear between the halves. However, the centerplane and cross-stream contours for an opposed row of crossed slots (Figs. 12(b), (f), and (g)) do not suggest any improvement in mixing over the corresponding circular hole case.

Conclusions

The following conclusions can be made from the results:

Transition liner curvature causes a drift of the jet trajectories toward the inner wall. The radial pressure gradient induced by the curvature inhibits the entrainment of the cross-flow by the inner wall jets and enhances that by the outer wall jets. This produces very different characteristics for the inner and outer wall jets.

Jet penetration and mixing in a curved and converging duct are similar to the effects seen in a converging straight channel, namely, that the optimum orifice spacing and momentum flux relationships are unchanged and the mixing is not inhibited by the convergence. This appears to be independent of whether the convergence in the curved duct is radial or circumferential.

Jet trajectories in a can (or annulus) are similar to those in a rectangular duct for the same jet-to-mainstream momentum-flux and orifice-spacing-to-duct-height (radius) ratios provided that the spacing is specified at the radius dividing the can (or annulus) into equal areas.

The mixing of jets from opposed rows of 45° slanted slots is similar, but slightly inferior, to that from equal area

holes. For aligned slots a bulk swirl is imparted to the flow, whereas when the slots on opposite walls are rotated 90°, opposite swirl is imparted on the top and bottom.

References

1. Reynolds, R., and White, C., "Transition Mixing Study Final Report," Garrett 21-5723, Garrett Turbine Engine Co., Phoenix, AZ, 1987 (NASA CR-175062).

2. Holdeman, J.D., Srinivasan, R., and Berenfeld, A., "Experiments in Dilution Jet Mixing," AIAA Journal, Vol. 22, No. 10, Oct. 1984, pp. 1436-1443.

3. Holdeman, J.D., and Srinivasan, R., "Modeling Dilution Jet Flowfields," Journal of Propulsion and Power, Vol. 2, No 1., Jan-Feb 1986, pp. 4-10.

4. Holdeman, J.D., et al., "Effects of Multiple Rows and Non-circular Orifices on Dilution Jet Mixing." Journal Of Propulsion and Power, Vol. 3, No. 3, May-June 1987, pp. 219-226.

5. Bruce, T.W., Mongia, H.C., and Reynolds, R.S.; "Combustor Design Criteria Validation, Vols. 1-3," AiResearch 75-211682(38), -1, -2, and -3, AiResearch Manufacturing Co., Pheonix, AZ, Mar. 1979.

6. Habib, M.A., and Whitelaw, J.H.; "The Calculation of Turbulent Flow in Wide Angle Diffusers," Numerical Heat Transfer, Vol. 5, No. 2, Apr.-June 1982, pp. 145-164.

7. Hughes, W.F., and Gaylord, E.W.; Basic Equations of Engineering Science, McGraw-Hill, NY, 1964.

8. Spalding, D.B., "A Novel Finite Difference Formulation for Differential Expressions Involving Both First and Second Derivatives." International Journal for Numerical Methods in Engineering, Vol. 4, No. 4, July-Aug. 1972, pp. 551-559.

9. Patankar, S.V., and Shih, T.M., Numerical Heat Transfer and Fluid Flow, McGraw-Hill, NY, 1980.

10. Patankar, S.V., and Spalding, D.B.; "A Calculation Procedure for Heat, Mass, and Momentum Transfer in Three-Dimensional Parabolic Flows," International Journal of Heat and Mass Transfer, Vol. 15, No. 10, Oct. 1972, pp. 1787-1806.

11. Launder, B.E., Reece, G.J., and Rodi, W.; "Progress in the Development of Reynolds Stress Turbulence Closure," Journal of Fluid Mechanics, Vol. 68, Pt. 3, Apr. 15, 1975, pp. 537-566.

12. Humphery, J.A.C., Taylor, A.M.K., and Whitelaw, J.H.; "Laminar Flow in a Square Duct of Strong Curvature." Journal of Fluid Mechanics, Vol. 83, Pt. 3, Dec. 5, pp. 509-527.

13. Chang, S.M., Humphery, J.A.C., and Modavi, A.; "Turbulent Flow in a Strongly Curved U-bend and Downstream Tangent of Square Cross-Sections," Physiochemical Hydrodynamics, Vol.4, No. 3, 1983, pp. 243-269.

14. Humphery, J.A.C., Whitelaw, J.H., and Yee, G., "Turbulent Flow in a Square Duct with Strong Curvature," Journal of Fluid Mechanics, Vol. 103, Feb. 1981, pp. 443-463.

15. Srinivasan, R., Berenfeld, A., and Mongia, H.C., "Dilution Jet Mixing Program, Phase I," GARRETT 21-4302, Garrett Turbine Engine Co., Phoenix, AZ, Nov. 1982, (NASA CR-168031).

16. Srinivasan, R. Coleman, E., and Johnson, K., "Dilution Jet Mixing Program, Phase II," GARRETT 21-4804, Garrett Turbine Engine Co., Phoenix, AZ, June 1984 (NASA CR-174624).

17. Lipshitz, A. and Greber, I.; "Dilution Jets in Accelerated Cross Flows," Ph.D. Thesis, Case Western Reserve University, Cleveland, OH, NASA CR-174717, June 1984.

18. Zizelman, James, "Dilution Jet Configurations in a Reverse Flow Combustor," M.S. Thesis, Case Western Reserve University, Cleveland, OH, (NASA CR-174888), Apr. 1985.

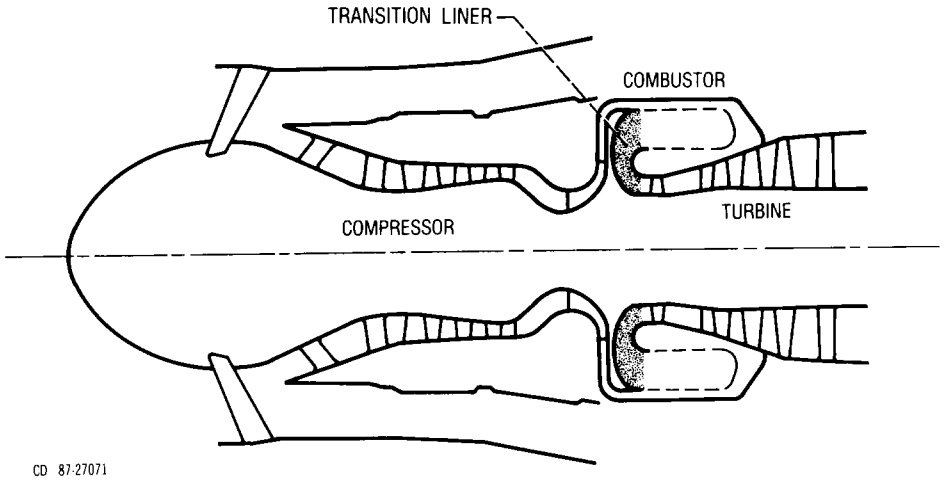

Fig. 1 Schematic of gas turbine engine with reverse-flow combustor configuration.

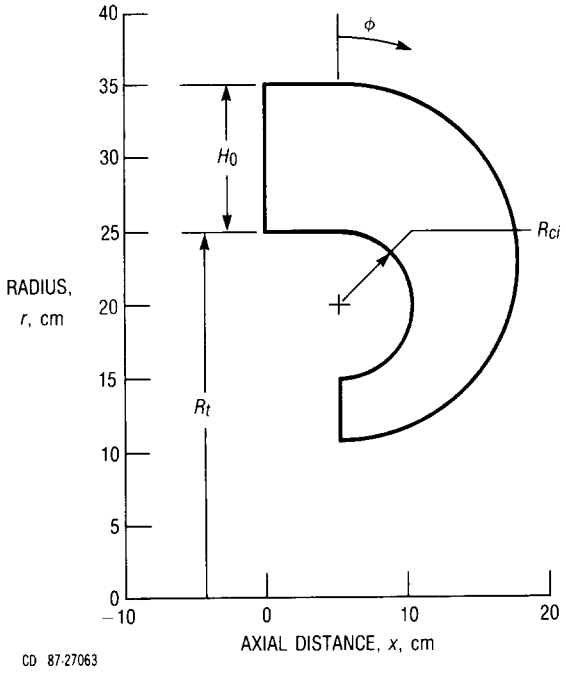

Fig. 2 Numerical experiment geometry.

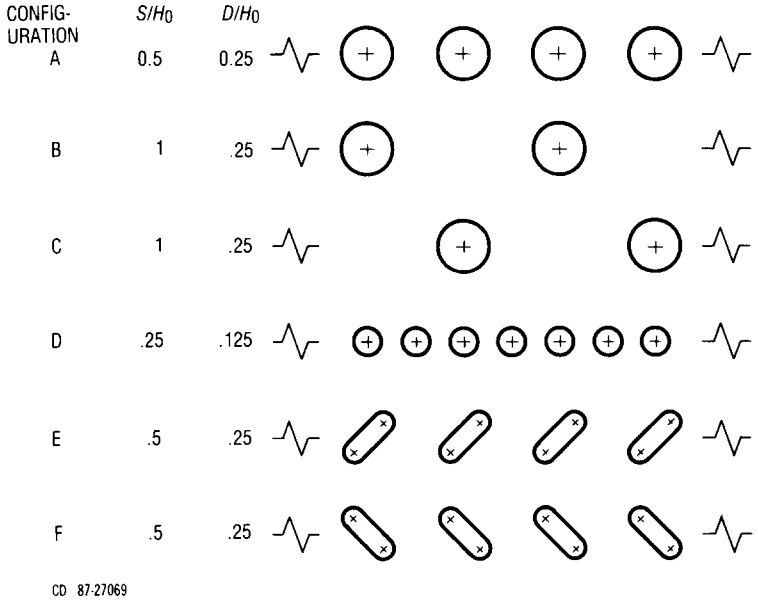

Fig. 3 Orifice configurations.

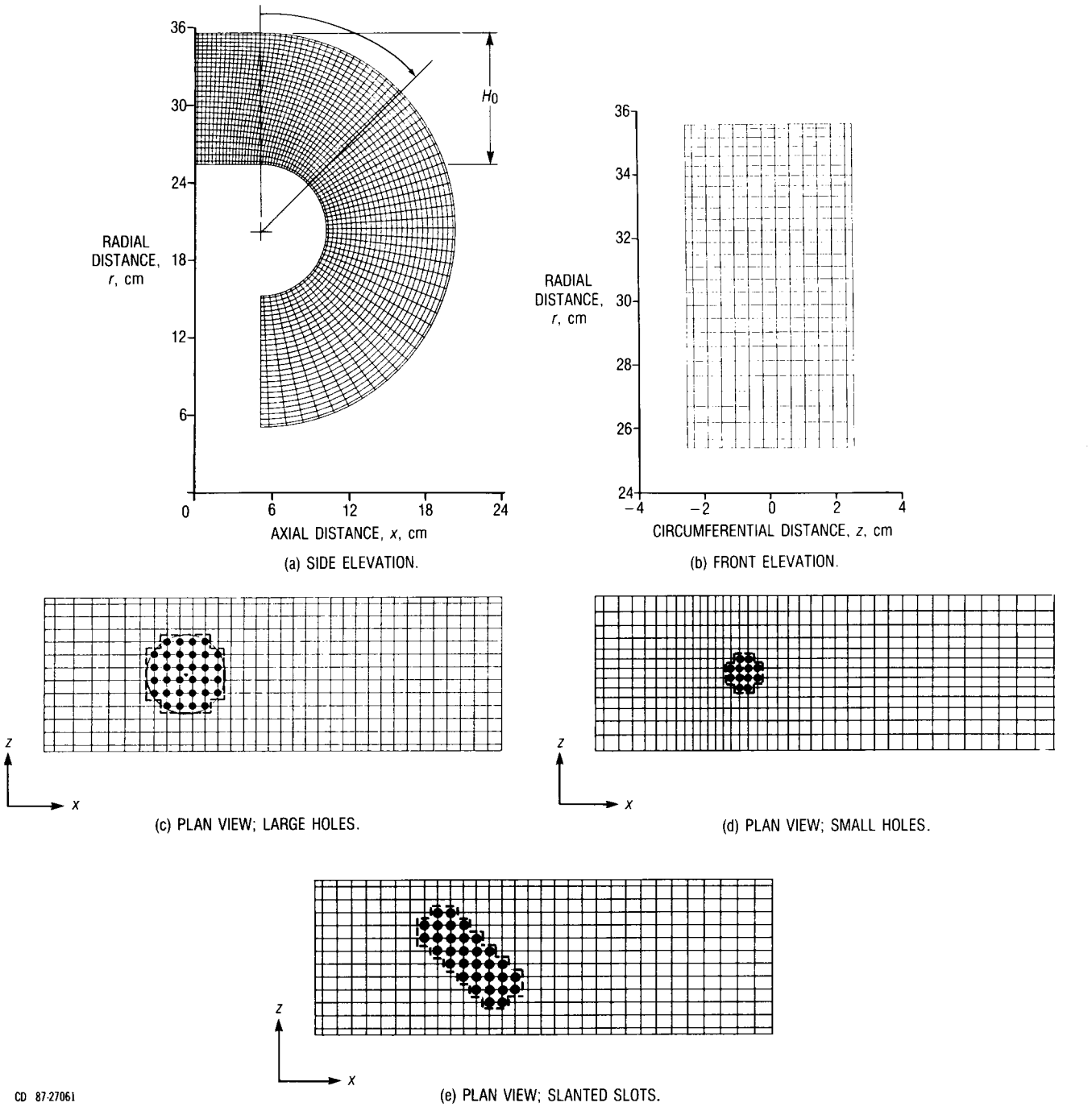

Fig. 4 Computational grid.

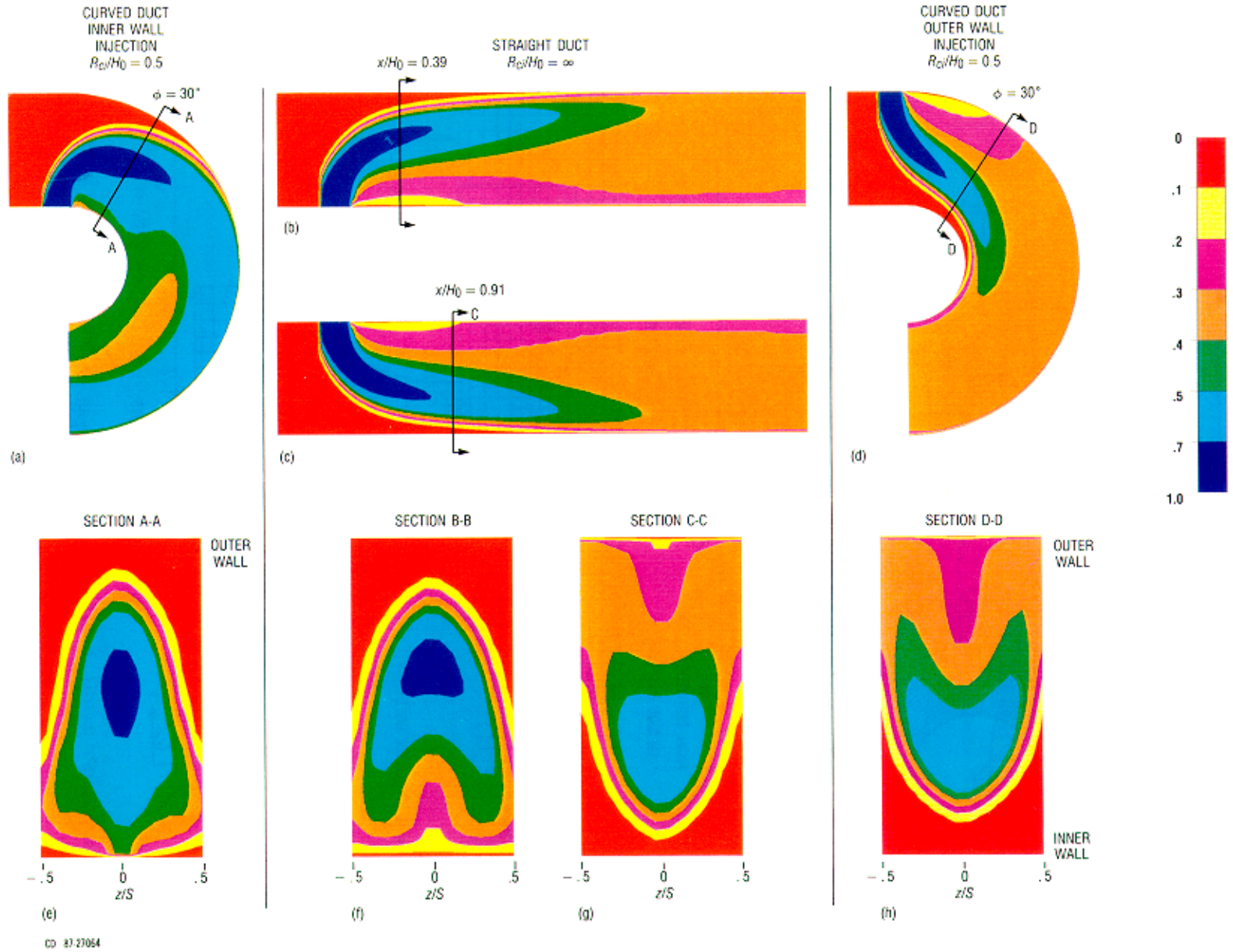

Fig. 5 Comparison of duct shapes and injection sites. All axial views at $z/S = 0$; $J = 26.4$, $S/H_0 = 0.5$, $D/H_0 = 0.25$; $R_t/H = \infty$.

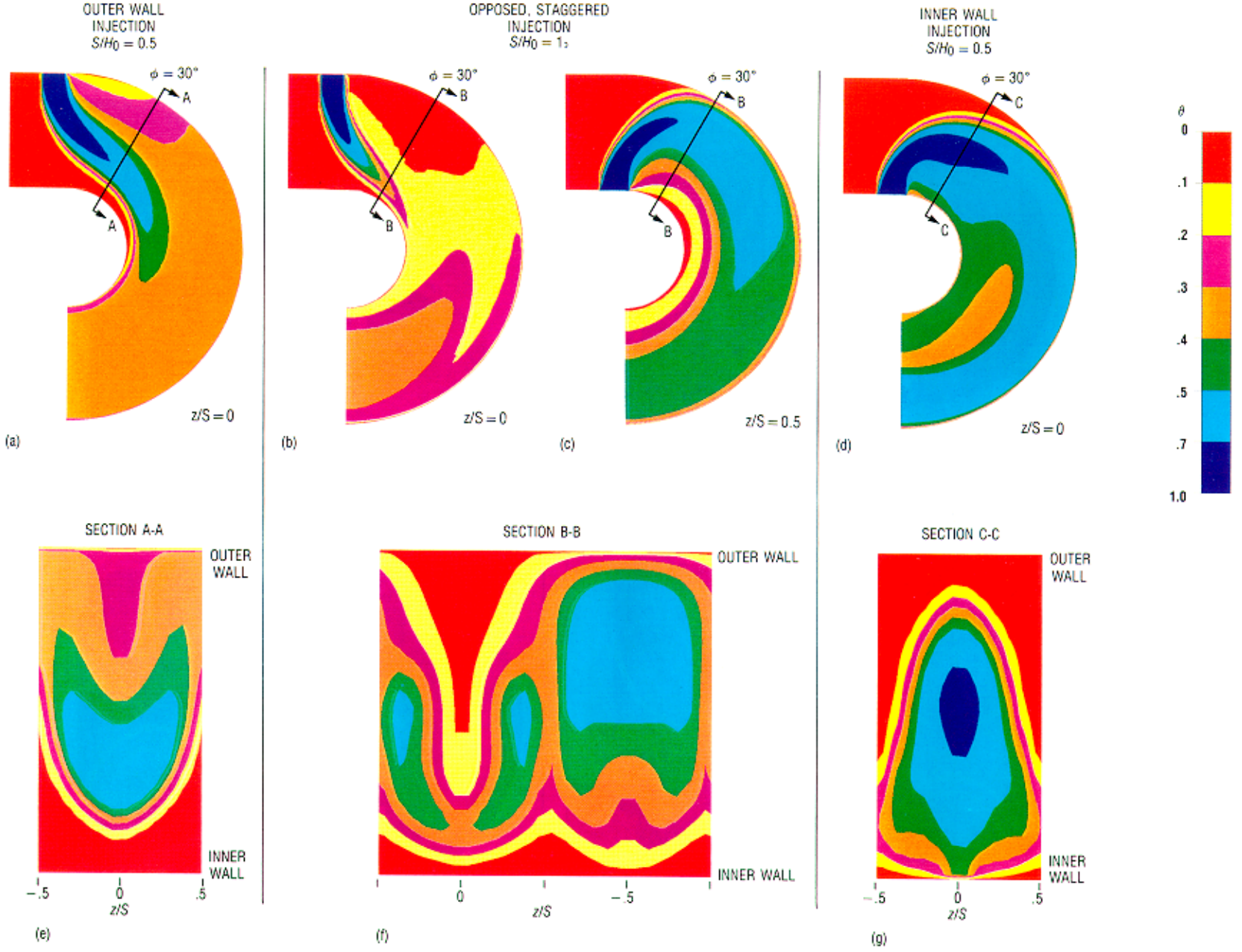

Fig. 6 Opposed rows with jet centerlines staggered. $J = 26.4$, $D/H_0 = 0.25$; $R_{ci}/H_0 = 0.5$, $R_t/H_0 = \infty$.

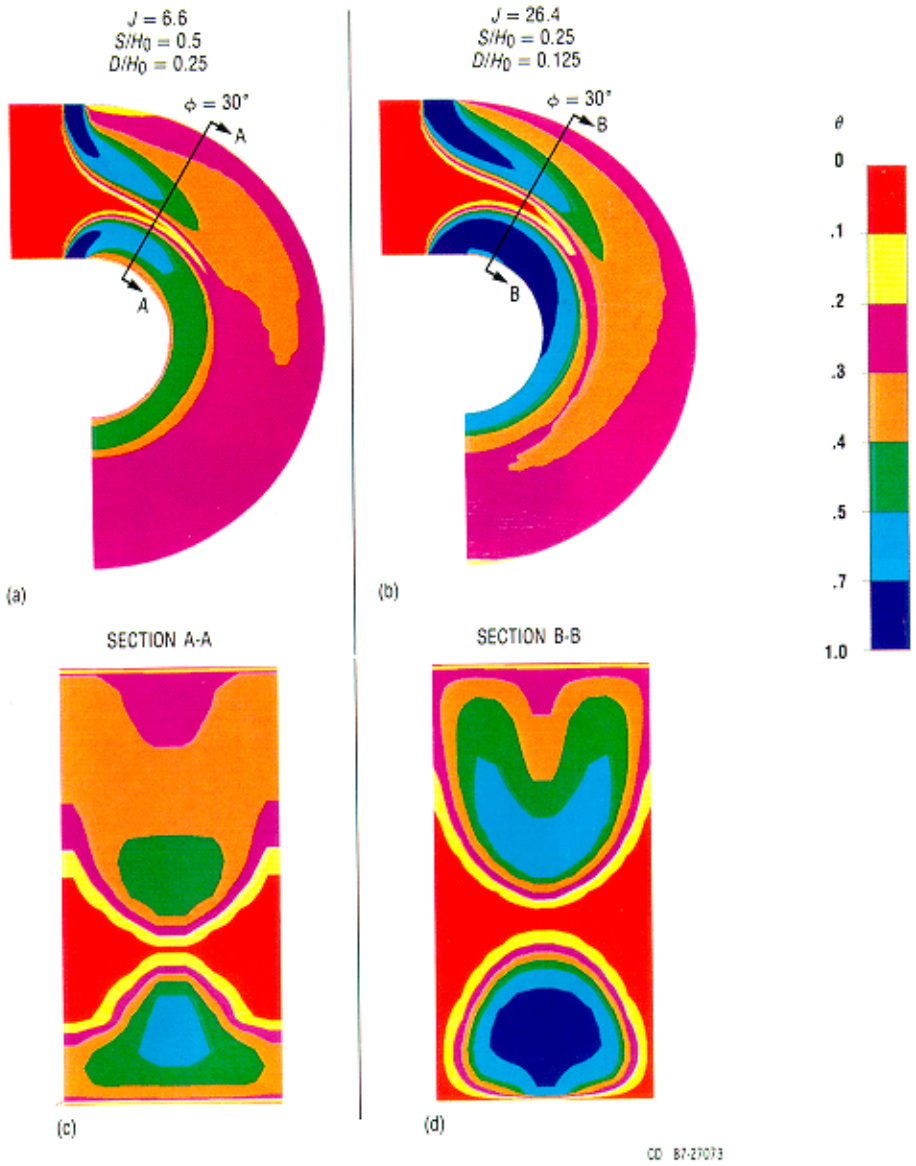

Fig. 7 Opposed rows with jet centerlines inline. All axial views at $z/S = 0$; $R_{ci}/H_0 = 0.5$, $R_t/H_0 = \infty$.

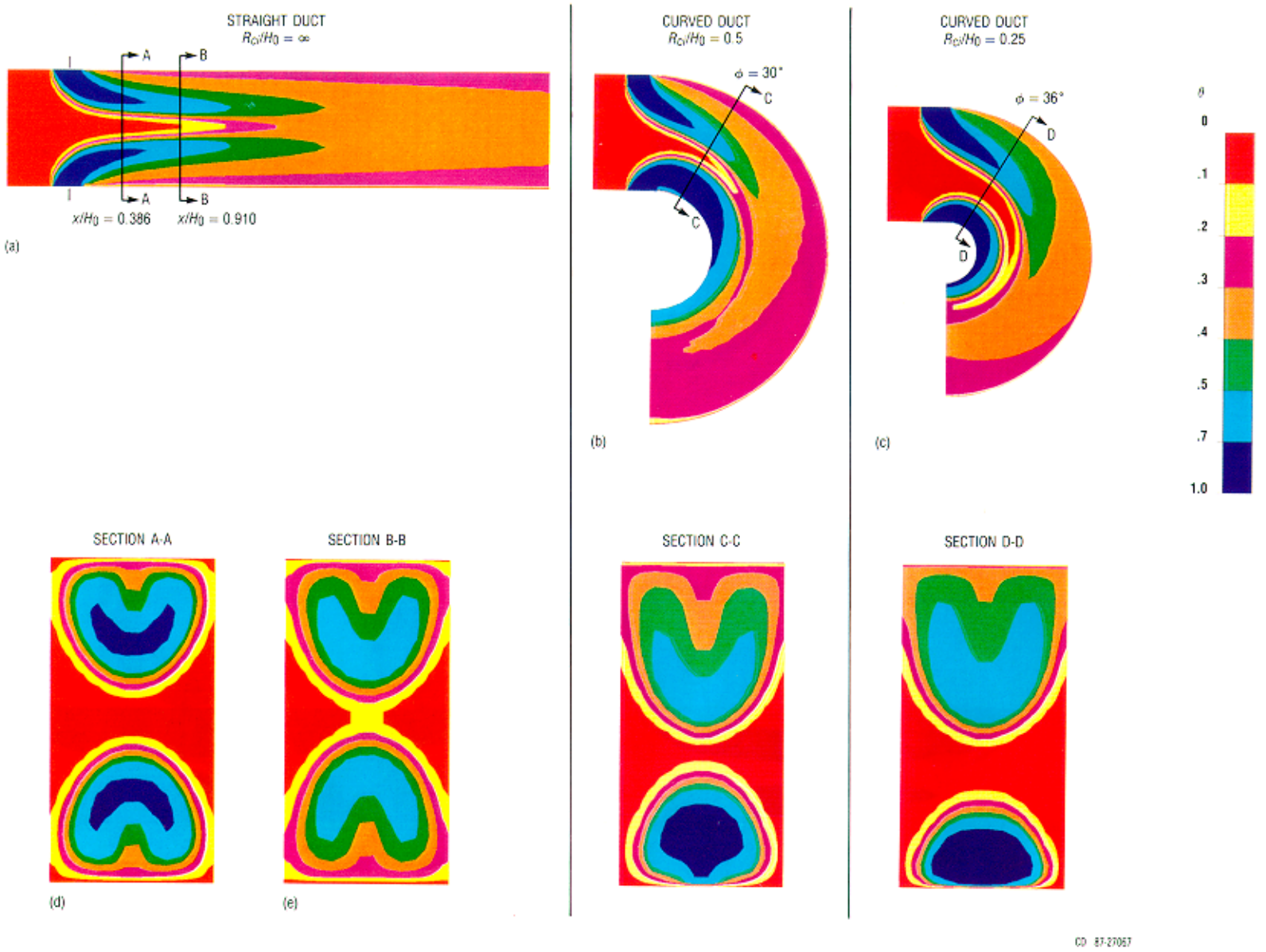

Fig. 8 Effect of radius of curvature in x-r plane. All axial views at $z/S = 0$; $J = 6.6$, $S/H_0 = 0.5$, $D/H_0 = 0.25$, $R_t/H_0 = \infty$.

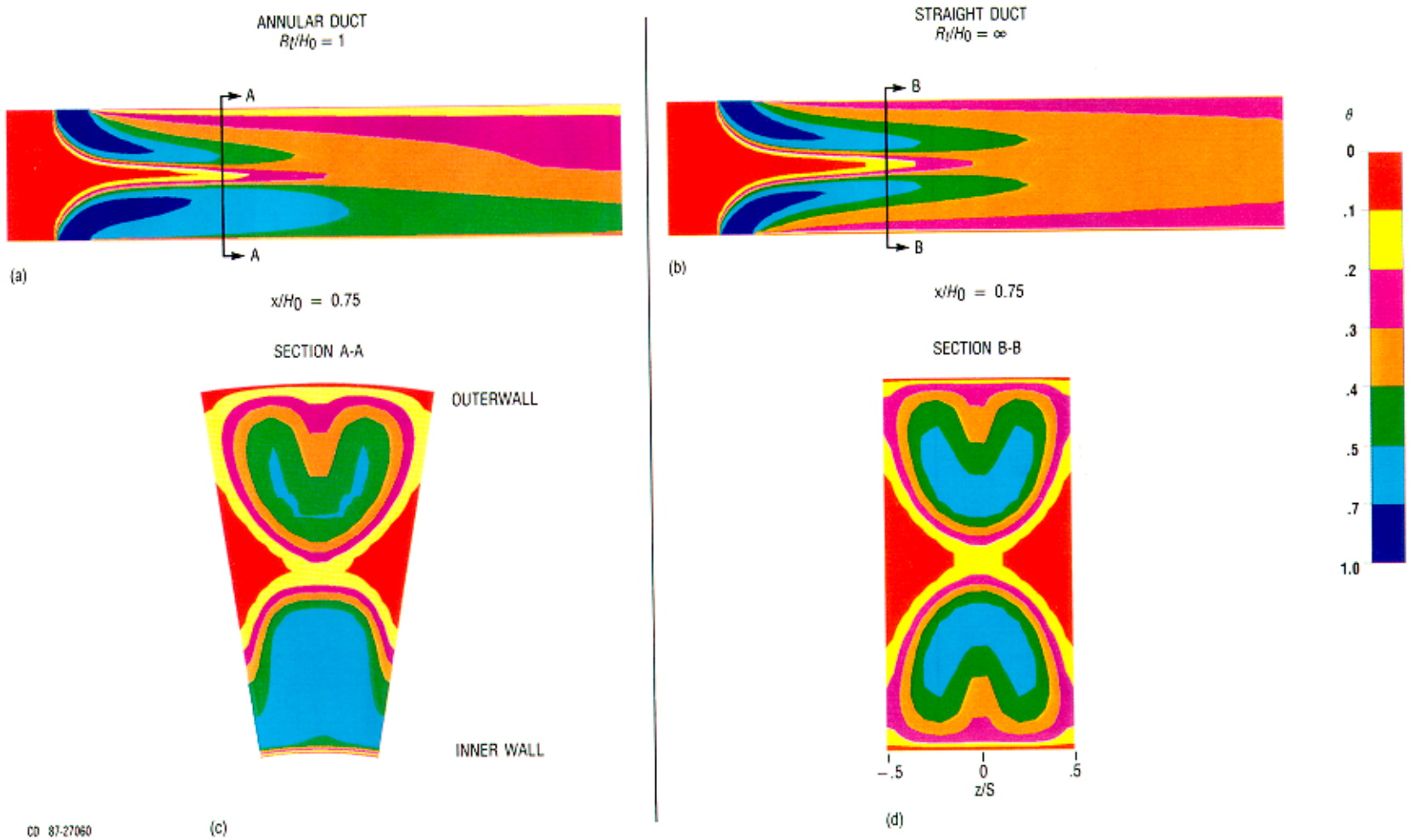

Fig. 9 Mixing of jets in an annular duct. All axial views at $z/S = 0$; $J = 6.6$, $S/H_0 = 0.5$, $D/H_0 = 0.25$, $R_{ci}/H_0 = \infty$.

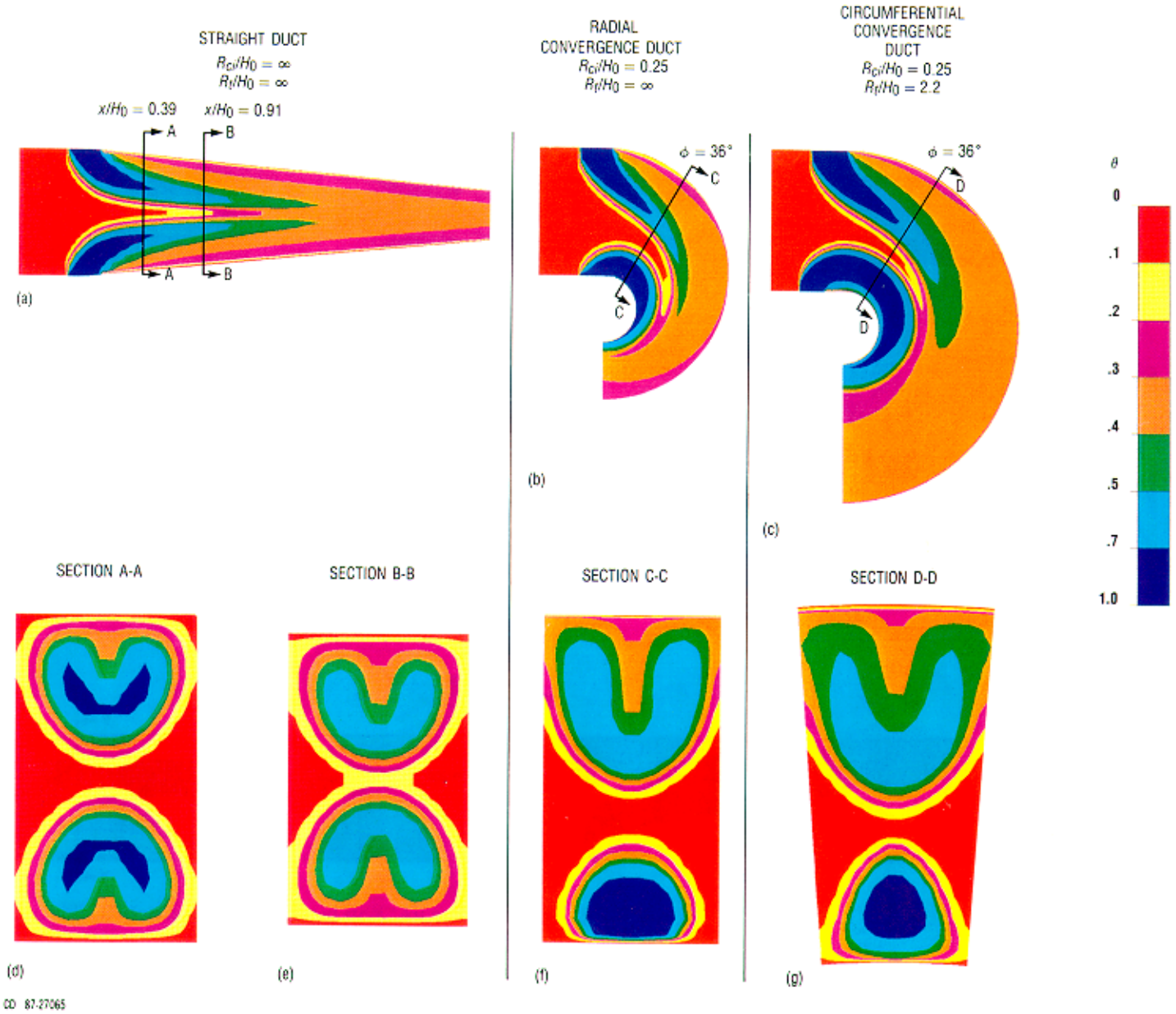

Fig. 10 Effect of convergence. Area ratio = 3:1; all axial views at $z/S = 0$; $J = 6.6$, $S/H_0 = 0.5$, $D/H_0 = 0.25$.

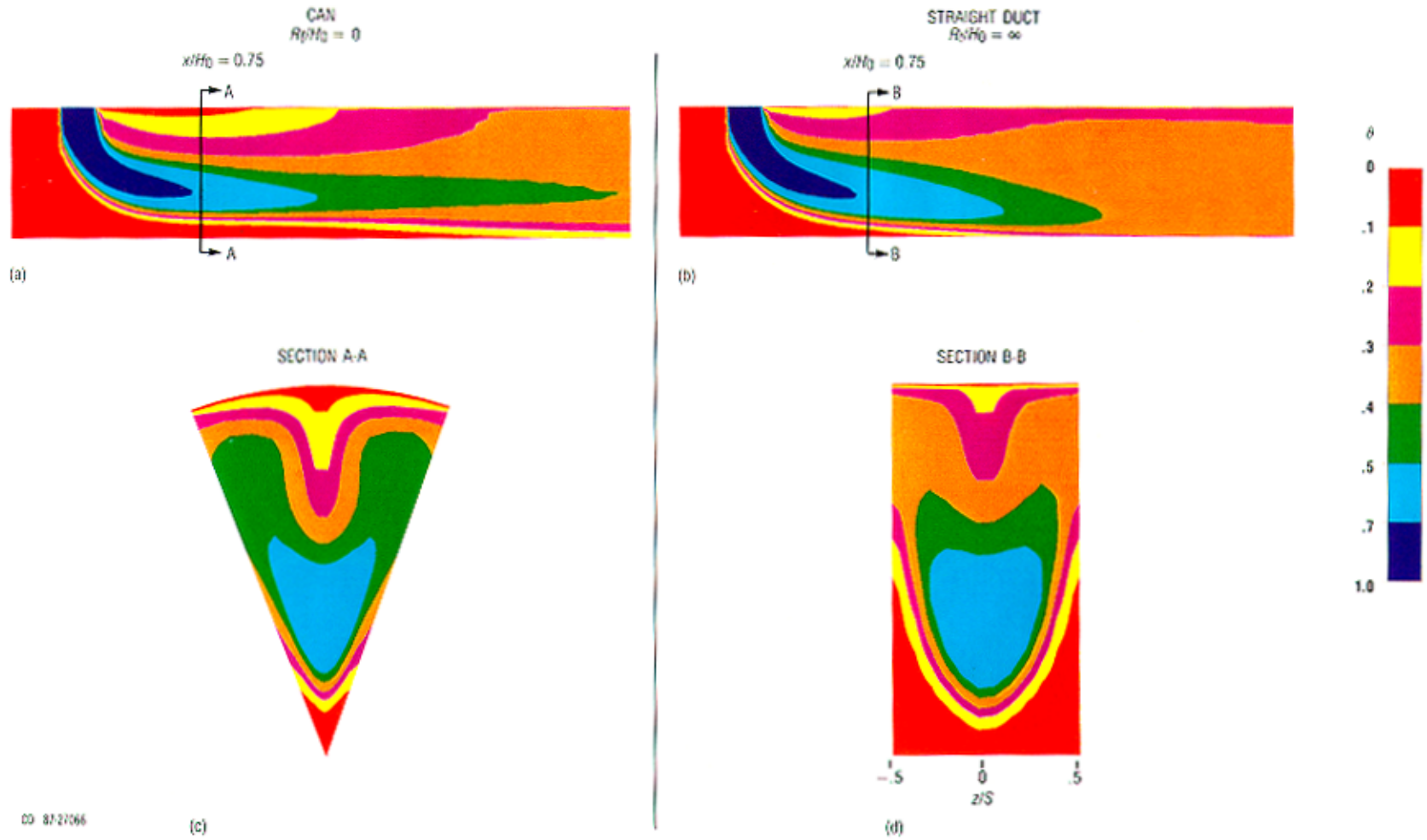

Fig. 11 Jets injected into can. All axial views at $z/S = 0$; $J = 26.4$, $S/H_0 = 0.5$, $D/H_0 = 0.25$, $R_{ci}/H_0 = \infty$.

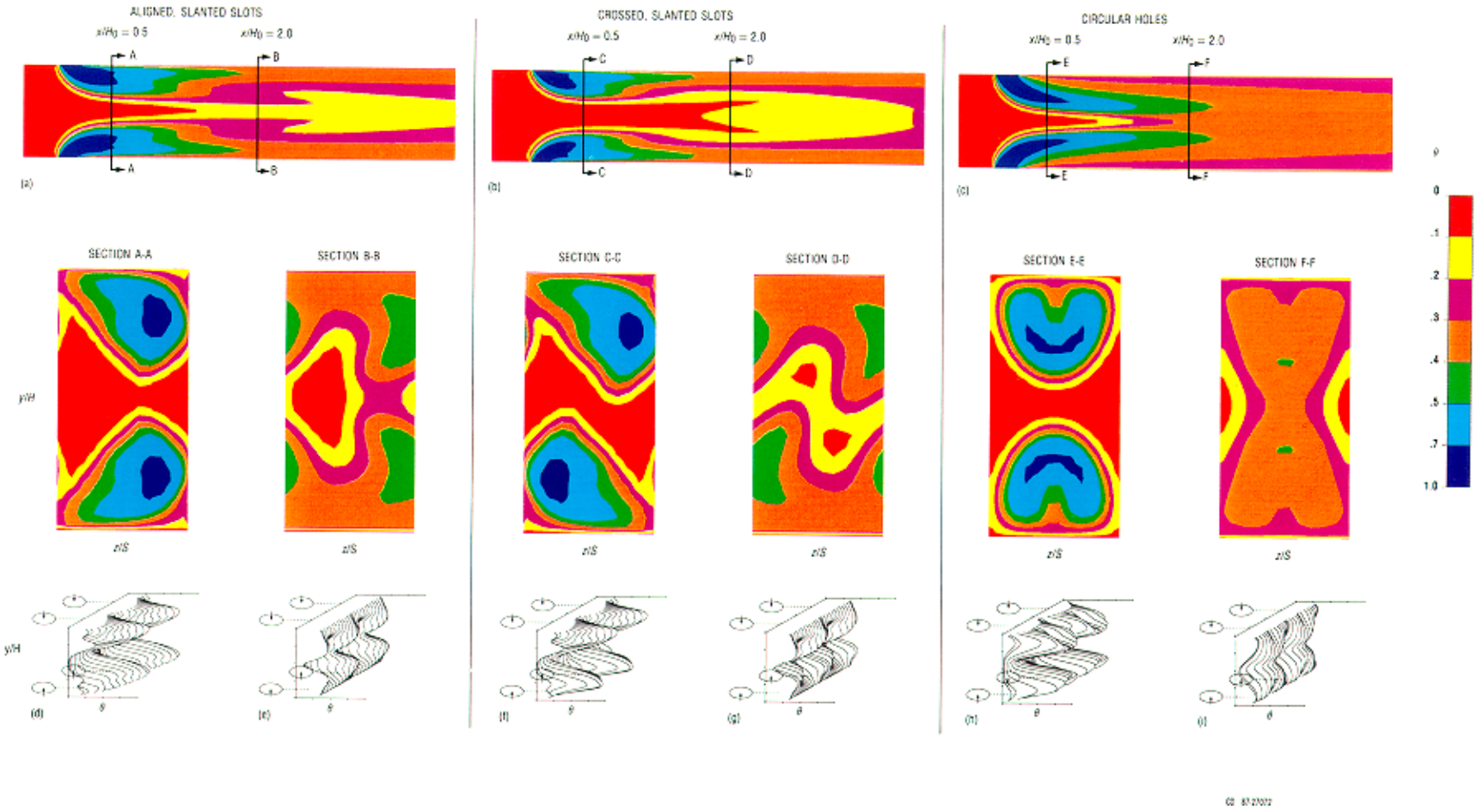

Fig. 12 Opposed rows of jets from slanted slots. All axial views at $z/S = 0$; $J = 26.4$, $S/H_0 = 0.5$, $D/H_0 = 0.25$, $R_{ci}/H_0 = \infty$, $R_t/H_0 = \infty$.

REPORT DOCUMENTATION PAGE

Form Approved
OMB No. 0704-0188

1. AGENCY USE ONLY (*Leave blank*)	2. REPORT DATE	3. REPORT TYPE AND DATES COVERED
	June 1987	Technical Memorandum

4. TITLE AND SUBTITLE

A Numerical Study of the Effects of Curvature and Convergence on Dilution Jet Mixing

5. FUNDING NUMBERS

WU–535–05–01–00

6. AUTHOR(S)

J.D. Holdeman, R. Reynolds and C. White

7. PERFORMING ORGANIZATION NAME(S) AND ADDRESS(ES)

National Aeronautics and Space Administration
Lewis Research Center
Cleveland, Ohio 44135–3191

8. PERFORMING ORGANIZATION REPORT NUMBER

E–3548

9. SPONSORING/MONITORING AGENCY NAME(S) AND ADDRESS(ES)

National Aeronautics and Space Administration
Washington, DC 20546–0001

10. SPONSORING/MONITORING AGENCY REPORT NUMBER

NASA TM–89878
AIAA–87–1953

11. SUPPLEMENTARY NOTES

Prepared for the 23rd Joint Propulsion Conference cosponsored by the AIAA, ASME, SAE, and ASEE, San Diego, California, June 29–July 2, 1987. J.D. Holdeman, NASA Lewis Research Center; R. Reynolds and C. White, The Garrett Turbine Engine Co., Phoenix, Arizona.

12a. DISTRIBUTION/AVAILABILITY STATEMENT

Unclassified - Unlimited
Subject Categories: 07

Available electronically at http://gltrs.grc.nasa.gov/GLTRS

This publication is available from the NASA Center for AeroSpace Information, 301–621–0390.

12b. DISTRIBUTION CODE

13. ABSTRACT ***(Maximum 200 words)***

An analytical program has been conducted to assemble and assess a three-dimensional turbulent viscous flow computer code capable of analyzing the flow field in the transition liners of small gas turbine engines. This code is of the TEACH type with hybrid numerics, and uses the power law and SIMPLER algorithms, an orthogonal curvilinear coordinate system, and an algebraic Reynolds stress turbulence model. The assessments performed in this study, consistent with results in the literature, showed that in its present form this code is capable of predicting trends and qualitative results. The assembled code was used to perform a numerical experiment to investigate the effects of curvature and convergence in the transition liner on the mixing of single and opposed rows of cool dilution jets injected into a hot mainstream flow.

14. SUBJECT TERMS

Dilution jet mixing; Transition liner; Gas turbine combustors

15. NUMBER OF PAGES

20

16. PRICE CODE

A02

17. SECURITY CLASSIFICATION OF REPORT	18. SECURITY CLASSIFICATION OF THIS PAGE	19. SECURITY CLASSIFICATION OF ABSTRACT	20. LIMITATION OF ABSTRACT
Unclassified	Unclassified	Unclassified	